Theor Chem Acc (1998) 100:241–252
DOI 10.1007/s002149800m37

Theoretical
Chemistry Accounts

Regular article

Ab initio correlation corrections to the Hartree-Fock quasi band-structure of periodic systems employing Wannier-type orbitals*

Martin Albrecht[1,2], **Peter Reinhardt**[1], **Jean-Paul Malrieu**[1]

[1]Université Paul Sabatier, Laboratoire de Physique Quantique Théorique, I. R. S. A. M. C.,
118 Route de Narbonne, F-31062 Toulouse Cedex, France
[2]Max-Planck-Institut für Physik Komplexer Systeme, Nöthnitzer Strasse 38, D-01087 Dresden, Germany

Received: 30 April 1998 / Accepted: 27 July 1998 / Published online: 7 October 1998

Abstract. A size-consistent ab initio formalism to calculate correlation corrections to ionization potentials as well as electron affinities of periodic systems is presented. Our approach is based on a Hartree-Fock scheme which directly yields local orbitals without any a posteriori localization step. The use of local orbitals implies non-zero off-diagonal matrix elements of the Fock operator, which are treated as an additional perturbation and give rise to localization diagrams. Based on the obtained local orbitals, an effective Bloch Hamiltonian is constructed to second order of perturbation theory with all third-order localization diagrams included. In addition, the summation of certain classes of diagrams up to infinite order in the off-diagonal Fock elements as well as the Epstein-Nesbet partitioning of the full Hamiltonian are discussed. The problem of intruder states, frequently encountered in many-body perturbation theory, is dealt with by employing the theory of intermediate Hamiltonians. As model systems we have chosen cyclic periodic structures up to an oligoethylene ring in double-zeta basis; however, the theory presented here straightforwardly carries over to infinite periodic systems.

Key words: Band structures – Perturbation theory – Bloch Hamiltonians – Localized orbitals – Intruder states

1 Introduction

In order to render ab initio correlation calculations on ground state properties as well as on excited states of large systems numerically accessible, numerous approaches have been explored during recent years. On molecules, a number of correlation methods have been formulated based on local and localized orbitals [1, 2], and experience has been collected for infinite periodic systems [3–6]. By the method of local increments [7], for example, correlated ground state properties of covalent [8–12] and ionic [13–16] systems have been obtained. A similar method has been explored to obtain correlation corrections [17, 18] to the valence band-structure. For polymers, correlated band-structure calculations have been presented recently by Förner et al. [19], based on localized Wannier orbitals, and we should mention the work of Borrmann and Fulde [20], where as further localization, in order to calculate a correlated band-structure, the bond-orbital approximation is employed. A completely different approach to correlated band-structure calculation has been established by Grobelsik [21] or Sun and Bartlett [22–24] which operates entirely in the reciprocal space.

The decisive aspect of the methods using localized orbitals in large systems is the considerable reduction of the excitation space to be taken into account in any configuration interaction (CI) procedure. This reduction is due to the local nature of the correlations. As an alternative to the frequent procedure of calculating canonical molecular orbitals (CMO) in the Hartree-Fock (HF) step and localizing them afterwards, it is also feasible to obtain orbitals which are already local as the result of the HF calculation. An approach along those lines, which has been proposed long ago [25], has been implemented recently [26–28] by some of the authors (and independently by Sano et al. [29]), and applied to molecules and ring systems. A somewhat different scheme to obtain localized orbitals with an entirely real-space approach has been proposed by Shukla [30–32].

The present paper being the third one in a series on ring molecules, we will henceforth denote [27] and [28] as papers I and II. The implementation described in these articles is used to obtain HF orbitals, and is the basis for the programming of the module used to calculate the

* Dedicated to Prof. Dr. Wilfried Meyer on the occasion of his 60th birthday

Correspondence to: M. Albrecht, Dresden

correlated band structures presented here. Since our model systems consist of cyclic periodic structures, the ionization potentials (IPs) and electron affinities (EAs) could be considered alternatively as the quasi band-structure of a periodic system. We will make use of the language of infinite periodic systems to give emphasis to this interpretation. Working with local HF orbitals requires taking into account the off-diagonal elements of the Fock operator which might be done in an iterative formulation [1, 6] or by incorporating those elements as an additional perturbation into the many-body perturbation theory (MBPT) [33]. Here we follow the second path, calculating in local HF orbitals an effective Bloch Hamiltonian to second order of perturbation theory with all third-order diagrams included which arise due to the off-diagonal elements in the Fock operator [referred to as localization diagrams, LMP2(3)]. We discuss the problem of intruder states frequently encountered in MBPT and propose several intermediate Hamiltonians to overcome the numerical difficulties pertaining to them. Where needed, particularly when some additional care has to be taken, the diagramatic formulation of the corresponding Bloch equations is made explicit. As model systems for the application of these Hamiltonians we use a $(C_2H_4)_{13}$ ring in minimal basis and a $(C_2H_4)_7$ ring in double-zeta (DZ) basis, using each time the geometry of polyethylene for the unit cell.

The paper is organized as follows: in Sect. 2 we give a short review of the theory of effective Hamiltonians (2.1), propose intermediate Hamiltonians (2.2), and discuss the possible inclusion of some infinite-order summations (2.3). In Sect. 3 we present our numerical results and Sect. 4 summarizes our conclusions.

2 Theory

2.1 Bloch equation for the effective Hamiltonian

Here we briefly give the main equations of the theory of effective Hamiltonians. A more detailed treatment was given by Lindgren and Morrison [34] and the theory has been rediscussed and enlarged by several authors [35–37]. The complete Hilbert space is thereby divided into a finite subspace P of dimension d, called the model space, and its orthogonal complement Q, as indicated by the corresponding projection operators:

$$P = \sum_{m=1}^{d} |m\rangle\langle m| \qquad Q = \sum_{\alpha} |\alpha\rangle\langle\alpha| \qquad P + Q = 1 \tag{1}$$

A wave operator Ω is constructed to yield d exact solutions Ψ^a of the full Hamiltonian H when operating on their projections Ψ_0^a onto the model space P, that means:

$$\Psi^a = \Omega\Psi_0^a \qquad (a = 1, \ldots, d) \tag{2}$$

where

$$\Psi_0^a = P\Psi^a, \qquad H\Psi^a = E^a\Psi^a \tag{3}$$

With these quantities an effective Hamiltonian H_{eff} is defined to recover the exact eigenenergies when operating on the projected functions Ψ_0^a in the model space according to:

$$H_{\text{eff}}\Psi_0^a = E^a\Psi_0^a \tag{4}$$

This Hamiltonian can be constructed from the wave operator Ω as

$$H_{\text{eff}} = PH\Omega P \tag{5}$$

Now the Bloch effective Hamiltonian is obtained with a wave operator which obeys the generalized Bloch equation

$$[\Omega, H_0] = (V\Omega - \Omega PV\Omega P) \tag{6}$$

where the Hamiltonian H has been partitioned into a zeroth-order Hamiltonian H_0 and a perturbation V. We comment on this later on. In a perturbative approach, Eq. (6) is calculated order by order, the first three orders being given by

$$[\Omega^{(1)}, H_0]P = QVP \tag{7}$$

$$[\Omega^{(2)}, H_0] = QV\Omega^{(1)} - \Omega^{(1)}PVP \tag{8}$$

and

$$[\Omega^{(3)}, H_0] = QV\Omega^{(2)}P - E^{(2)}\Omega^{(1)} \tag{9}$$

Once the wave operator is calculated, the effective Hamiltonian is given by Eq. (5), where the application of H causes the effective Hamiltonian to be one order higher than the corresponding wave operator. Provided that the basis used is orthonormal, the terms appearing in Eqs. (5), (7) and (8) can be evaluated in normal form by means of Wick's theorem and might be represented by Goldstone diagrams [34]. Up to this point the theory is straightforward, all diagrams which we took into account being given in the appendix. It should be noted, however, that the second term in Eq. (8) gives rise to so-called backfold diagrams. We would like to point out that in the construction of $\Omega^{(2)}$ no exclusion-principle-violating (EPV) diagrams should be included, as is usually done to cancel the last term in Eq. (9).

In keeping with our desire to calculate correlation corrections to the excited states, the theory is applied as explained in the following for the case of particles, the hole case being completely equivalent. The HF calculation provides orthonormal and local occupied as well as virtual orbitals, denoted by a, b, c and r, s, t, respectively. To denote the elements of the effective Hamiltonian, μ and η will be used instead of r, s, t. With the application to periodic systems in mind, each such index comprises a cell index, an orbital index, and a spin index. From these orbitals, the model space P is constructed to contain the $(N+1)$-electron determinants $c_r^\dagger|\Psi_{\text{scf}}\rangle$ created from the HF ground state $|\Psi_{\text{scf}}\rangle$ by adding a particle to the orbital r

$$P = \sum_r c_r^\dagger|\Psi_{\text{scf}}\rangle\langle\Psi_{\text{scf}}|c_r \tag{10}$$

The orthogonal complement Q is approximately given by the single and double excitations applied to the model space, specifically

$$\begin{aligned} Q = &\sum_{a,s,r} c_s^\dagger c_a c_r^\dagger|\Psi_{\text{scf}}\rangle\langle\Psi_{\text{scf}}|c_r c_a^\dagger c_s \\ &+ \sum_{a,b,s,t,r} c_t^\dagger c_s^\dagger c_b c_a c_r^\dagger|\Psi_{\text{scf}}\rangle\langle\Psi_{\text{scf}}|c_r c_a^\dagger c_b^\dagger c_s c_t \end{aligned} \tag{11}$$

The entire Hamiltonian H is split into the zeroth-order Hamiltonian H_0 and the perturbation $V = H - H_0$. As zeroth-order Hamiltonian we take the diagonal of the Fock operator F in the model space

$$H_0 = \sum_r F_{rr} \qquad F_{rr} = \langle r|F|r\rangle \qquad |r\rangle = c_r^\dagger|\Psi_{\text{scf}}\rangle \tag{12}$$

Consequently, as mentioned above, the off-diagonal elements will appear as an additional perturbation with respect to the case of the treatment in CMOs, where F is diagonal and $H_0 = F$.

In the following applications we calculate the effective Hamiltonian to second order in perturbation theory and include all the third-order diagrams, which contain at least one off-diagonal Fock matrix element as additional perturbation due to the localization. Henceforth, these diagrams are referred to as localization diagrams; we abbreviate this level of theory by LMP2(3).

The Bloch effective Hamiltonian being in general non-hermitian, it is symmetrized by

$$\frac{\langle\mu|H_{\text{eff}}|\eta\rangle + \langle\eta|H_{\text{eff}}|\mu\rangle}{2} \tag{13}$$

To order the excited states, each of them will be associated with a quasi wavenumber k, labeling its irreducible representation of the group of rotations of the ring system considered; k plays the same role as the wavenumber used in infinite periodic systems, but is a discrete quantity for finite cyclic systems. To this end, the effective Hamiltonian is rewritten with explicit indices

$$|\mu\rangle = |\sigma_\mu, o_\mu, \mathbf{R}_\mu\rangle \tag{14}$$

where the spin variable σ_μ is taken to be $+\frac{1}{2}$ (and is omitted henceforth), thus applying the usual approximation of spin degenerate excited states. The vectors $\mathbf{R}_\mu$ denote the unit cell where the orbital o_μ is located. Where the notation is clear, we will write simply μ instead of o_μ. Exploiting the rotational symmetry of a cyclic periodic system allows us to keep one cell index always in the reference cell **0**, so that

$$(H_{\text{eff}})^{\mathbf{R}}_{\mu,\eta} = \langle\mu\mathbf{0}|H_{\text{eff}}|\eta\mathbf{R}\rangle \tag{15}$$

These matrix elements can be considered as representing a hopping of an electron from orbital μ located in cell **0** to an orbital η in cell **R**. In finite cluster approaches to solid state band structures, these matrix elements are extracted from molecular type calculations [17, 18], whereas here the complete system is considered. Having obtained the quantity $(H_{\text{eff}})^{\mathbf{R}}_{\mu,\eta}$, we follow the same procedure as depicted by Gräfenstein et al. [17, 18], i.e. the real space matrix is transformed into the quasi reciprocal space k by virtue of

$$H_{\mu\eta}(\mathbf{k}) = \sum_{\mathbf{R}} \mathrm{e}^{\mathrm{i}\mathbf{k}\mathbf{R}} \langle\mathbf{0}\mu|H|\eta\mathbf{R}\rangle \tag{16}$$

where the index "eff" has been omitted. Diagonalization in the (quasi) reciprocal space yields the eigenfunctions and eigenenergies. Save for this last trivial step, all calculations are done in real space, particularly no summation or integration in the reciprocal space are needed at any step of the procedure.

2.2. Intruder states and intermediate Hamiltonians

MBPT suffers from the problem of intruder states, as has been pointed out and discussed by several authors [37, 38]. In general they are due to a strong coupling between the model space P and the outer space Q. This coupling will take place if two states which are similar in energy belong to the two different spaces. In the framework of the theory employed here, this is easy to see. A diagram such as the one in Fig. 1 represents in the lower part the operator sequence QVP, where a state $|\eta\rangle \in P$ is mixed by the perturbation V with the determinant $c_r^\dagger c_a |t\rangle \in Q$. The formula corresponding to this diagram in the notation of the appendix is

$$\sum_{art} \frac{(t\eta|ra)}{\Delta_{tr}^{a\eta}} \sum_{s} \frac{(\mu t|as)F_{sr}}{\Delta_{ts}^{a\eta}} \tag{17}$$

where the denominator

$$\Delta_{tr}^{a\eta} = \epsilon_a + \epsilon_\eta - \epsilon_t - \epsilon_r = \epsilon_\eta - (\epsilon_t + \epsilon_r - \epsilon_a) \tag{18}$$

invoked by the commutator in the Bloch equations represents the energy difference between the two states in P and Q, respectively,

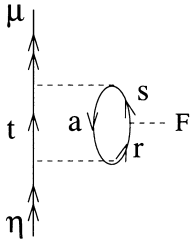

Fig. 1. A diagram which might give rise to the problem of intruder states

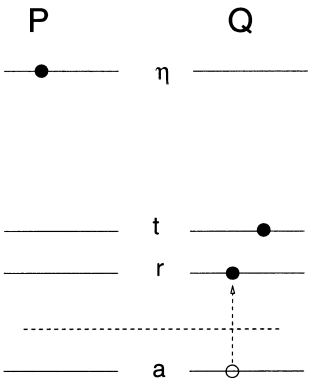

Fig. 2. A sketch of energy levels which cause a vehement coupling between the spaces P and Q in the evaluation of the diagram in Fig. 1

and might lead to numerical convergence problems in the case depicted in Fig. 2, where the energy of $|\eta\rangle$ is already as high as the energy of $c_r^\dagger c_a |t\rangle$, resulting in a minute energy denominator. One solution to the problem consists in simply ignoring the high-energy states. For many practical cases this should cause no problems, since those states, well separated from the lower ones, should not contribute much to the correction of the lower conduction bands or EAs, respectively. In fact, Bartlett and co-workers proposed the same procedure in their reciprocal-space approach when encountering this problem, giving a formula for the critical energy, beyond which the states in the model space are neglected (Eq. 47 in [22]). For the cases studied in this work, this turned out to be sufficient. However, from a theoretical point of view it seems favorable to have a procedure at hand which treats those cases more rigorously.

The theory of intermediate Hamiltonians [35–37] strives to avoid the strong coupling between the model space P and the excitations contained in Q, splitting the model space into a main model space P_{m} and an intermediate space P_{i}. In the case at hand, P_{m} will contain the low-lying excitations, while the troublesome high-energy states as $|\eta\rangle$ in Fig. 2 will be placed in the intermediate space.

The intermediate Hamiltonian is now constructed by means of an additional wave operator R to give only exact energies in the main model space, the energies being placed in the intermediate space losing their strict physical significance. The equations corresponding to Eqs. (2), (3), (4), and (5) are, with $P = P_{\text{m}} + P_{\text{i}}$

$$\Psi^a = R\bar{\Psi}_0^a \qquad (a = 1, \ldots, d_{\text{m}}) \tag{19}$$

$$\bar{\Psi}_0^a = P\Psi^a, \qquad H\Psi^a = E^a\Psi^a \tag{20}$$

$$H_{\text{int}}\bar{\Psi}_0^a = E^a\bar{\Psi}_0^a \tag{21}$$

$$H_{\text{int}} = PHRP \tag{22}$$

For the construction of R we choose

$$PRP = P \tag{23}$$

and are left with the principal equation

$$QRP_{\text{m}} + QRP_{\text{i}}\Omega P_{\text{m}} = Q\Omega P_{\text{m}} \tag{24}$$

It should be noted that Ω is now defined as before, but with respect to P_{m} with dimension $d_{\text{m}} < d$ instead of the entire model space P.

As discussed by Heully et al. [37], one can conceive different choices for the term QRP_{i}. In the following we look at two cases, called case I and case II, translate the corresponding Bloch equations into the necessary diagrams, and point out their merits with respect to the construction of an effective Hamiltonian.

Case I employs the simple choice

$$QRP_{\text{i}} = 0 \tag{25}$$

leading to the Bloch equation

$$Q[R,H_0]P_\mathrm{m} = Q(V\Omega - \Omega V\Omega)P_\mathrm{m} \tag{26}$$

It is immediately evident from Eq. (26) and Fig. 1 that the intruder state problem is suppressed this way by virtue of the operator P_m on the right-hand side of Eq. (26) which excludes states with too high an energy ($|\eta\rangle$) in the diagram in Fig. 1. It should be noted, however, that in this way the intermediate Hamiltonian is rendered strongly non-hermitian, since P_m excludes to the right, i.e. at the bottom of the diagrams, the part P_i of the model space.

Case II constructs consequently also the part QRP_i, leading to [37] the coupled equations

$$Q[R,H_0]P_\mathrm{m} = Q\big(V\bar{\Omega} - \bar{\Omega}V\bar{\Omega}\big)P_\mathrm{m} - QRP_\mathrm{i}[\Omega,H_0]P_\mathrm{m} \tag{27}$$

$$Q[R,H_0]P_\mathrm{i} = Q\big(V - \bar{\Omega}V\big)P_\mathrm{i} \tag{28}$$

$$\bar{\Omega} := (P_\mathrm{m} + Q)\Omega \tag{29}$$

Again, there is a partial suppression of the states in P_i which manifests itself in the definition of $\bar{\Omega}$. Also the operator P_m to the right has evidently the same effect as discussed above. However, in the presence of intruder states, the second equation will again introduce numerical divergencies. They are avoided by repartitioning the Hamiltonian as proposed by Heully

$$\tilde{H}_0 = H_0 + P_\mathrm{i}WP_\mathrm{i} \tag{30}$$

$$= (P_\mathrm{m} + Q)H_0 + \sum_i \epsilon_i |i\rangle\langle i| \tag{31}$$

The additional perturbation W acts only in the intermediate space, and it can be easily checked that the substitution

$$\tilde{V} = V - W \tag{32}$$

will not affect Eqs. (27) and (28), yielding

$$Q\big[R,\tilde{H}_0\big]P_\mathrm{m} = Q\big(V\bar{\Omega} - \bar{\Omega}P_\mathrm{m}V\bar{\Omega}\big)P_\mathrm{m} - QRP_\mathrm{i}\big[\Omega,\tilde{H}_0\big]P_\mathrm{m} \tag{33}$$

$$Q\big[R,\tilde{H}_0\big]P_\mathrm{i} = Q\big(V - \bar{\Omega}P_\mathrm{m}V\big)P_\mathrm{i} \tag{34}$$

$$\bar{\Omega} := (P_\mathrm{m} + Q)\Omega \tag{35}$$

However, care has to be taken when treating the waveoperator Ω with this partitioning. Rewriting Eq. (6) with P replaced by P_m results in

$$\big[\Omega,\tilde{H}_0\big]P_\mathrm{m} = ((V - W)\Omega P_\mathrm{m} - \Omega P_\mathrm{m}V\Omega P_\mathrm{m}) \Longleftrightarrow \tag{36}$$

$$\big[\Omega,\tilde{H}_0 - W\big]P_\mathrm{m} = (V\Omega P_\mathrm{m} - \Omega P_\mathrm{m}V\Omega P_\mathrm{m}) \tag{37}$$

so Ω still has to be calculated with $H_0 = \tilde{H}_0 - W$. Having conveniently shifted the energies of the intermediate space this way, the coupling between P_i and Q poses no problem any more. We now turn to a discussion of the modifications necessary in the diagrams of the effective Hamiltonian, and the additional diagrams needed which appear here for the first time.

The effect of the operator P_m to the right of a term and at the bottom of a diagram has been emphasized already. Secondly, the omission of P_i in $\bar{\Omega}$ leads via the term $QV\bar{\Omega}P_\mathrm{m}$ to a suppression of the type of diagrams represented by the first diagram of Fig. 3, where Ω is followed by a state in P_i. The same term gives rise to the omission of the class of diagrams depicted by the second diagram in Fig. 3, where the second-order operator leads into the intermediate space, whereas exclusively the Q space is admitted. As for the rest of the diagrams, no special care has to be taken as long as the classification of the states by P_m and P_i and the shift due to the operator W are taken into account. However, the diagrams so far do not represent the novel term $-QRP_\mathrm{i}[\Omega,H_0]P_\mathrm{m}$ in Eq. (33) and (34), which reads for the intermediate wave operator to second order $R^{(2)}$

$$-QR^{(1)}P_\mathrm{i}\Big[\Omega^{(1)},\tilde{H}_0\Big]P_\mathrm{m} \tag{38}$$

The corresponding diagram is given in Fig. 4 and should be evaluated according to Eq. (38) instead of applying the usual evaluation rules, which would lead to wrong energy denominators. The correct result is

$$-\sum_{artT}\frac{(\mu t|ra)(Tt|ar)F_T\eta\Delta^\eta_{T^*}}{\Delta^{a\eta}_{tr}\Delta^{aT^*}_{tr}\Delta^\eta_T} \tag{39}$$

In particular the commutator in Eq. (38) gives rise to an energy numerator $\Delta^\eta_{T^*} = \epsilon_\eta - \epsilon_{T^*}$ where the asterisk at the index of the intermediate state T indicates that the shifted energy is to be used. In contrast to this, the energy denominator Δ^η_T originating from the operator $\Omega^{(1)}$ must be constructed with the unshifted energy as discussed above (Eq. 37). Having thus circumvented the coupling between P_i and Q, we conclude by remarking that the partitioning of the model space might introduce also a strong coupling between P_i and P_m, which is present both in case I and in case II, the latter being manifest by the energy denominator Δ^η_T in Eq. (39). This possible coupling is usually resolved by diagonalizing the entire model space. In our case this might lead to a blurring of the so-far localized orbitals. Alternatively, the operator $\Omega^{(1)}$ can be adjusted by a 2×2 matrix diagonalization of the two mixing states [39, 40].

Having proposed a method to treat the intruder states, we like to emphasize that they do not only pose a purely technical obstacle or a convergence problem, but have also a physical aspect. If one considers for instance the photoelectron ionization (PES) spectrum, the mixing between 1-hole and 2-hole–1-particle states (2h–1p) is a physical phenomenon. It is well known in molecular physics, where from the forth IP onward the Koopman's states (essentially 1-hole) remain usually identifiable as intense peaks, but are embedded into a forest of non-Koopman's or satellite states, which are essentially of 2h–1p character and of weaker intensity. Of course, all eigenstates are a mixing of 1h and 2h–1p single determinants, since they interact through the bielectronic Hamiltonian. One may say that the 2h–1p state spreads the 1h states by mixing with them and taking a part of their absorption intensity [41, 42]. Going to extended periodic systems (through finite systems) increases this mixing process. The correspondance between the PES spectrum and a distribution of essentially 1h states can only be seen as a simplification. When one leaves the Fermi level toward higher energies, all eigenstates have mixed 1h and 2h–1p character, and the study of the exact density of states would become a very demanding task due to this extent and density of near degeneracies originating from the electronic correlation, i.e. the bielectronic nature of H.

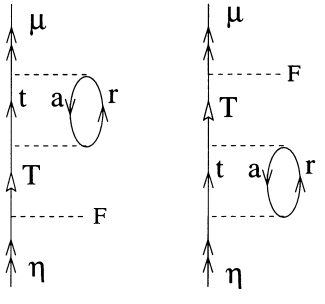

Fig. 3. Diagrams which represent interactions passing through the intermediate space (denoted as T) at the bottom (*left side*) and at the top (*right side*)

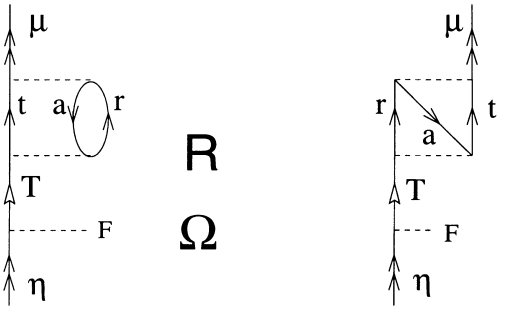

Fig. 4. The only diagram representing Eq. (38) together with its exchange partner

Our procedure, which sacrifices the details of the mixing between 1h and 2h–1p determinants, can be seen as an approximate way to approach the "band spectrum" after correlation. The use of a strictly degenerate zeroth-order picture avoids the appearance of vanishing (and positive) energy denominators in the perturbation expansion once intermediate Hamiltonians are used, i.e. masks the nondegeneracy effects which we would face, if we were using Bloch functions. Our procedure gives some information of a rather virtual 1h spectrum responsible for the photoemission which should be broadened by a more accurate calculation of the effect of 2h–1p states. Except for the region of the Fermi level, the perturbative calculation employing Bloch functions would become intractable. Employing localized orbitals, i.e. introducing the delocalization after the correlations of the effective Fock-matrix elements, can be seen as a trick to escape this dilemma. However, one should bear in mind the approximate character of this procedure.

2.3 Infinite order summations

Some special higher-order diagrams can be summed up to infinite order without any increase in the computational effort, provided that no additional summation indices are introduced. We first concentrate on summing certain classes of diagrams by repeatedly adding the perturbation due to the off-diagonal Fock-matrix elements. Adding just one element F_{sr} to the diagram in Fig. 1 results in changing also an index for the Coulomb perturbation of this particular third-order diagram, whereas adding another F_{rs} element restores the sequence of r and s for the integrals and leads to an additional factor

$$\frac{F_{rs}F_{sr}}{\Delta_{ts}^{a\eta}\Delta_{tr}^{a\eta}} \tag{40}$$

The summation obtained by the series of diagrams with $1, 3, 5, \ldots, (2n+1)$ Fock elements as indicated in Fig. 5 leads to the following correction of Eq. (17)

$$\sum_{arts} \frac{(t\eta|ra)(\mu t|as)F_{sr}}{\Delta_{tr}^{a\eta}\Delta_{ts}^{a\eta} - F_{sr}^2} \tag{41}$$

Similarly, diagrams with $2, 4, \ldots, 2n$ Fock elements can be summed over to give

$$\sum_{arts} \frac{(t\eta|ra)(\mu t|ar)F_{sr}^2}{\left(\Delta_{tr}^{a\eta}\Delta_{ts}^{a\eta} - F_{sr}^2\right)\Delta_{tr}^{a\eta}} \tag{42}$$

We would like to point out that a naive correction of all the diagrams in the appendix would lead erroneously to diagrams which do not correspond any more to the Bloch equations of Eq. (6).

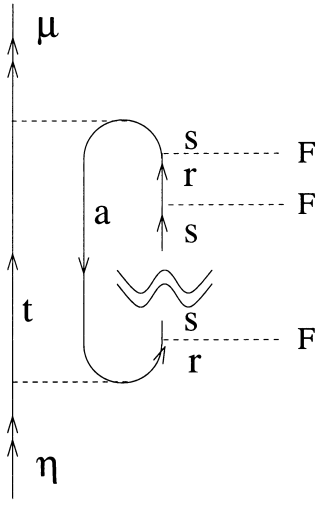

Fig. 5. The type of diagram obtained by adding pairwise Fock-matrix elements to the diagram in Fig. 1. The *doubly waved line* indicates the infinite series of Fock elements

Rather, the construction of the diagrams of higher orders have to be derived carefully from those equations. Specifically, to construct an infinite series based on the backfold diagram in Fig. 16 of the Appendix, the origin of the underlying terms like *...PVPVPVPVP* has to be derived by successive insertion of the Bloch equations order by order. For example, inserting Eq. (7) in Eq. (8) yields

$$[\Omega^{(2)}, H_0] = QV\boxed{QVP} - \boxed{QVP}PVP \tag{43}$$

where the last term gives rise to the backfold diagram of Fig. 16. Note that it is essential to keep in mind how the wave operators have been inserted in order to get the energy denominators right. In Eq. (43) $\Omega^{(1)}$ is marked by a box so as to trace it back. The third-order equation

$$[\Omega^{(3)}, H_0] = QV\Omega^{(2)}P - \Omega^{(2)}PVP - \Omega^{(1)}PV\Omega^{(1)}P \tag{44}$$

is thus transformed, using Eq. (7) and Eq. (43), into

$$\begin{aligned}\left[\Omega^{(3)}, H_0\right] = {} & QV\boxed{QV\boxed{QVP} - \boxed{QVP}VP} \\ & - \boxed{QV\boxed{QVP} - \boxed{QVP}VP}\,PVP \\ & - \boxed{QVP}\,PV\boxed{QVP}\end{aligned} \tag{45}$$

The second term contains in its second part a sequence

$$\boxed{\boxed{QVP}VP}\,PVP \tag{46}$$

and is at the origin of the series we are looking for. From the construction it can be seen that each further term $PVP = PFP$ gives a factor (-1), and that the backfold character is kept, so that the 3-F diagram in this series is given by Fig. 6. Note that there is no such series related to the diagrams four and six of Fig. 16, since the repetition of the state $|\mu\rangle$ would go through the P-space, an event which is not allowed by the Bloch equations without changing the diagram type by invoking backfold diagrams.

The same kind of summation was used for the ground-state energy calculations in papers I and II ([27] and [28]). Additionally the Epstein-Nesbet (EN) corrections [43] were applied, using the diagonal of the exact Hamiltonian H as zeroth-order Hamiltonian H_0 rather than the diagonal of the Fock operator F, i.e.

$$H_0 = \sum_i |i\rangle\langle i|H|i\rangle\langle i| \tag{47}$$

We use $|i\rangle = c_r^\dagger|\Psi_{\mathrm{scf}}\rangle$ when i denotes a particle state and $|i\rangle = c_a|\Psi_{\mathrm{scf}}\rangle$ when i runs over the occupied orbitals. This simply changes the energy denominators, as for example in the case of Fig. 1 and Eq. (17) with the abbreviations $J_{ar} = (aa|rr)$, $K_{ar} = (ar|ar)$ as

$$\Delta_{rt}^{a\eta} \to \Delta_{rt}^{a\eta} + J_{ar} - K_{ar} + J_{at} - K_{at} - J_{rt} + K_{rt} \tag{48}$$

This result is nothing else than an infinite summation of certain classes of diagrams as it was shown above for the summation of Fock-matrix elements. As an example, the left side of Fig. 7

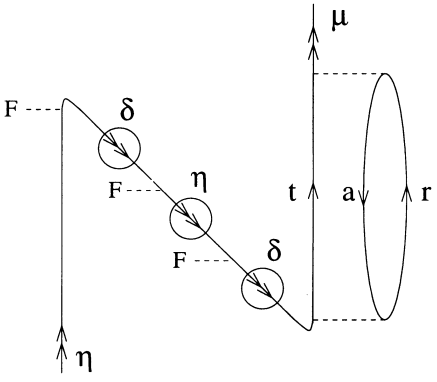

Fig. 6. This fifth-order diagram forms part of the infinite series of Fock-operator insertions to the backfold diagram in Fig. 16.

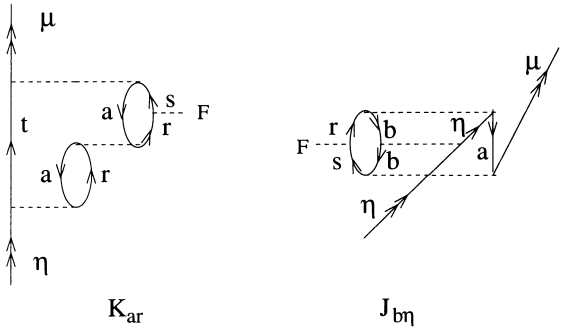

Fig. 7. Addition of further interaction lines to some third-order diagrams. The additional line is the one in the middle, giving rise to K_{ar} (*left diagram*) and $J_{b\eta}$ (*right diagram*)

displays the diagram of Fig. 1 with one additional interaction line, giving rise to the factor

$$\frac{K_{ar}}{\Delta_{tr}^{a\eta}} \tag{49}$$

which gives as summation series together with the denominator $\Delta_{tr}^{a\eta}$ in the prefactor (Eq. 17) an overall denominator

$$\Delta_{tr}^{a\eta} - K_{ar} \tag{50}$$

in agreement with Eq. (48). A similar suggestion had been put forth by Yaris [44]. We note however, that contrarly to the case of the ground-state energy calculation, not all terms can be rigorously obtained this way. For example, the additional interaction line shown in the second diagram of Fig. 7 introduces an energy denominator which is absent in the original diagram without that interaction line. Despite this fact, which is closely linked to the non-hermiticity of the effective Bloch Hamiltonian, we stuck to the first point of view of the EN formulation as given in Eq. (47). We thus favor a somewhat more hermitian Hamiltonian. This decision should be without loss of generality and is similar to prefering case II over case I in Sect. 2.2

3 Numerical results

To demonstrate the feasibility of our approach, we performed calculations on two $(C_2H_4)_n$ rings as cyclic periodic test systems. The unit cell (C_2H_4) was taken to be the unit cell of polyethylene in the geometry used by König and Stollhoff [45], i.e. $r_{C-C} = 0.1536$ nm, $r_{C-H} = 0.1083$ nm, $\angle_{C-C-C} = 112.7°$, and $\angle_{H-C-H} = 106.8°$. Details of the algorithm employed to obtain the HF solution in local orbitals and examples of applications both for HF and for correlation calculations are given in papers I and II ([27] and [28]).

3.1 Effective Hamiltonians: LMP2(3)

In this section the effective Bloch Hamiltonian was constructed using the Møller-Plesset (MP) perturbation theory to third order in the sense discussed above. The deep–lying states originating from the 1*s* orbitals of the carbon atoms as well as states with rather high energies have been ignored to avoid the problem of intruder states to be dealt with in Sect. 3.3 In the cases treated here this does not imply a significant loss of accuracy, as is also shown in Sect. 3.3

To begin with, the influence of the number of neighbors of the central unit cell taken into account during the correlation calculation on the final result is investigated to find reasonable cut-off criteria. In a first step, only excitations within the central unit cell itself were used in the correlation calculation. Next, the two next-nearest neighbors were added to the correlation range. The process had been continued until convergence on the results was achieved. The most pronounced advantage of our direct-space approach and the use of local orbitals consists in the fact that the contribution of excitations involving orbitals separated by up to a distance d is supposed to decrease rapidly with d. If this is the case, as it is expected in covalent and ionic systems, a cut-off radius R can be defined beyond which the correlation space does not need to be taken into account, thus rendering correlation calculations for large and even infinite periodic systems accessible and feasible. To ensure that the distance decreases with the increasing number of the coordination sphere of the central cell, a rather large ring is chosen. Specifically, we calculated the excitation spectrum for a $(C_2H_4)_{13}$ ring in minimal all-electron basis. Figure 8 displays our HF results. Since the system is finite, the spectrum is discrete; however, a quasi wavenumber k is used as explained above to arrange the levels in bands as is done for extended systems, the group theoretical arguments being the same for both cases. This correspondence is made explicit by the notation on the abscissa in Fig. 8. Note that the X-point is never exactly reached in finite systems with an odd number of unit cells, as we present them here. For 13 unit cells we have thus seven irreducible k-points, the highest index being at 12/13 of the full interval $\Gamma - X$. The figure (Fig. 8) shows the six valence levels together with the lowest two conduction levels. Figure 8 also contains the HF results of infinite polyethylene (calculated with CRYSTAL [47]) with the same unit cell geometry and the same basis set as used for the ring

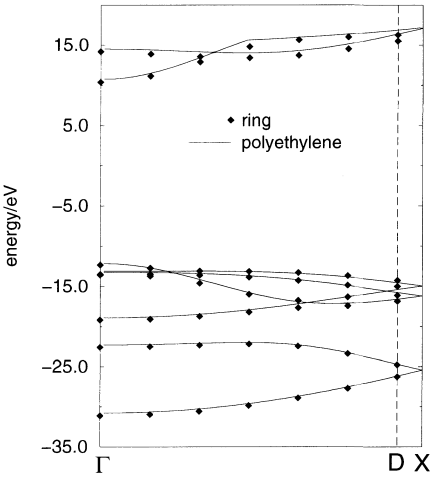

Fig. 8. Hartree-Fock (HF) spectrum for the $(C_2H_4)_{13}$ ring in a minimal basis. Displayed are the six valence lines and the lowest two conduction lines. The data are indicated by *diamond symbols*. The HF result for the corresponding infinite system, polyethylene, is shown by the *solid lines*. For the finite ring the k-values extend up to $D = \frac{12}{13}X$

calculations. Thus, despite the discrete nature of the ring problem and the minimal basis employed, the "band-structure" of the ring already reveals the characteristic features of a full periodic calculation, and can be well compared to that published by Karpfen [46].

We proceed by calculating an effective Hamiltonian to third order in the sense discussed above. Figure 9 shows the results for the calculations concerning two of the upper valence lines where excitations within one, three, and five cells had been allowed. The corresponding data are represented by long dashed, dashed, and dotted lines, respectively. The HF result has been added as solid lines. To keep the graph simple, only two of the four lines at the top of the valence spectrum are shown. A comparison between the calculations with the cut-off range of one neighboring cell (dashed lines) and those where a cutoff radius of two cells has been applied (dotted lines) allows us to conclude that it is sufficient to confine the excitation space to the central cell together with the first neigbor to the left and right. This cutoff range has been used throughout the remainder of this work.

Next a somewhat smaller $(C_2H_4)_7$ ring has been considered. Again the geometry of polyethylene was used for the unit cell as before. However, the basis is now the DZ basis of Huzinaga [48], which was used with slight modifications in the calculations of Karpfen [46] as well as in the work of König and Stollhoff [45] concerning polyethylene. In our work we employed Huzinaga's 7*s*3*p* set contracted to 4*s*2*p* for the C atom without scaling factors and his 4*s* set contracted to 2*s* at the H atom [48]. In Fig. 10 the HF results (solid lines) are compared to the overall LMP2(3) results obtained with an effective Hamiltonian (dotted lines) and Fig. 11 depicts in more detail the correlation corrections for two of the upper valence lines (bottom panel) and the two lowest conduction lines (top panel). The contributions of the second and third order are indicated as dashed and dotted lines, respectively. The discrete k values are marked with symbols for some of the lines. The overall effect consists in a shift of the levels towards the gap. In the case of the valence lines, Fig. 11 shows in its lower part that the third-order localization diagrams [MP(3)] bear a significant part of that shift, whereas in the case of the conduction levels the role of the third-order localization contribution is a pure squeezing of the lines. This can be seen by comparing the MP2 results (dashed) with the MP2(3) data (dotted) in the upper part of Fig. 11. The overall MP(3) contribution amounts to 5–10% of the second-order effect.

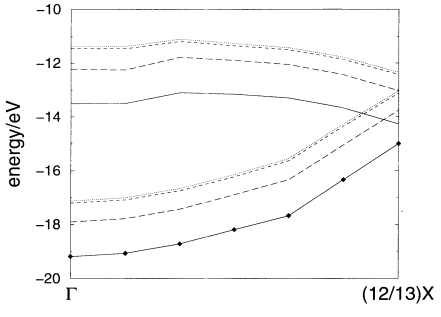

Fig. 9. Two of the four upper valence lines for the $(C_2H_4)_{13}$ ring. The *solid lines* repeat the HF results of Fig. 8, whereas the *long-dashed*, *dashed*, and *dotted lines* display the third-order corrections LMP2(3) with one, three and five cells being correlated, respectively

3.2 Effective Hamiltonian with infinite summations and EN corrections

Still sticking to the effective Bloch Hamiltonian, the infinite-order summations in the Fock-matrix elements as well as the EN corrections are applied. Firstly, the additional contribution of the EN correction with respect to the MP results is compared in the second order. Figure 12 displays the results of MP2 (long dashed) for two of the upper valence lines with the EN-corrected data to second order (EN2, dashed). Clearly, the EN approach gives a remarkable correction.

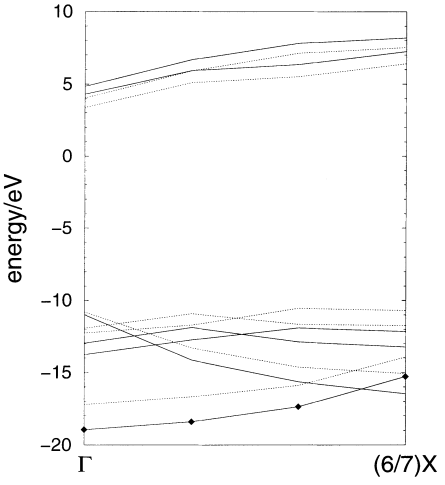

Fig. 10. The upper four valence lines and lower two conduction lines of the $(C_2H_4)_7$ ring are displayed as *solid lines* for the HF results and *dotted lines* for the LMP2(3) correlation corrections

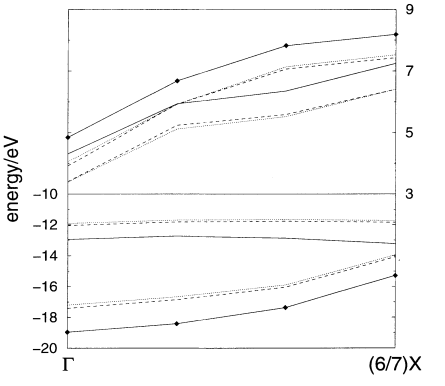

Fig. 11. The two lowest conduction lines (*upper panel*) as well as two of the four highest valence lines (*lower panel*) of the $(C_2H_4)_7$ ring are depicted on HF level (*solid lines*). They are corrected to second order (LMP2) as indicated by the *dashed lines* and with third-order localization diagrams included [LMP2(3)] as shown by the *dotted lines*

The contribution of the third-order localization diagrams with MP might be added to the EN2 results. This is depicted by the dotted lines. From this it is evident that the EN2 approach gives an additional correlation contribution to the MP2 results (dashed versus long dashed line in Fig. 12) which is even more pronounced than the contribution of the third-order corrections with MP theory (dotted versus dashed line).

The ground-state energy as well as the upper two IP (indexed "1" and "2") and the lowest two EA (indexed "3" and "4") at the points Γ and $\frac{6}{7}X$ in the "Brillouin zone" are compared for the different levels of the theory in Table 1. Also shown is the "gap" as the difference *LUMO* − *HOMO* which happens to be located at the Γ-point. For the EN results the change with respect to the HF calculations is added as a percentage. The overall change brought about by LMP2 with respect to HF can be estimated from these data to be around 10%. The second-order results are in turn augmented by the third-order localization contribution by an average of again 10%. Taking into account infinite-order summations of some classes of localization diagrams (column "$MP + F^{\infty}$" in Table 1) adds again almost the same amount. Furthermore, the EN results in second order have an even more pronounced effect with respect to ordinary MP2 than the MP(3) corrections. Finally, the results of the EN approach for the third-order diagrams together with the infinite-order summation of certain classes of localization diagrams are given in the last column of Table 1. They lead once more to a more pronounced third-order effect. In fact, the results for the correlated ground-state energy mirrors these tendencies. It should be pointed out that in this work the weight is put on the comparison between the different methods employed rather than on the presentation of state-of-the-art calculations. Our overall reduction of the gap of 16% is certainly limited by the basis set (DZ). For the case of polyacetylene, Sun and Bartlett [22] have carefully analyzed the basis-set dependence of the band gap and reported a reduction of 16.7% using a STO-3G basis versus 40.4% with a DZP basis. However, they applied MBPT(2) in the reciprocal space using canonical orbitals, which corresponds in our approach to taking into account all localization diagrams to infinite order. In this respect, our reduction of 16% seems reasonable in its order of magnitude. Since we dealt with oligoethylene in a middle-sized basis only, we do not strive to enter into the present controversy regarding polyacetylene. Just for the sake of completeness we note that Förner et al. [19] performed band-structure calculations on polyacetylene as well, using a local approach; however, their results do not coincide with the results of Sun and Bartlett and neither with those of Suhai [49, 50]. For the ground-state energy of polyethylene, correlation corrections are made available by König and Stollhoff [45], obtained by employing more elaborate correlation methods involving finite cluster approximations. They obtain a correlation energy of 0.2922 au; Suhai reported 0.3042 with a 6-31G** basis [51].

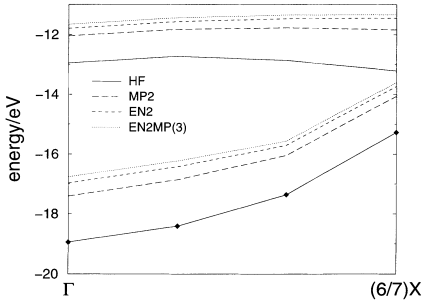

Fig. 12. The correlation corrections to second order (LMP2) for two of the upper valence lines are represented (*long-dashed lines*) and compared to the Epstein-Nesbet (EN) results in the same order, i.e. EN2 (*dashed lines*). The additional effect of the ordinary localization diagrams LMP(3) is indicated for the sake of comparison (*dotted*)

3.3 Intermediate Hamiltonians

As pointed out in Sect. 2.2, taking into account particles with high energies might give rise to intruder states. The

Table 1. Ground-state energy E_0 (in Hartree) and the energies (in eV) of the upper two valence levels (indexed "1" and "2") and the lower two conduction levels (indexed "3" and "4") at the Γ point and at the point $\frac{6}{7}X$, for the different levels of theory. Note that at the X-point the levels 1 and 2, 3 and 4, are degenerate. The gap (contained in the last line) is the difference $\epsilon_3(\Gamma) - \epsilon_2(\Gamma)$. For the Epstein-Nesbet (EN) quantities the change with respect to the Hartree-Fock (HF) results is indicated in parentheses

		Second order		Third order on top of		
				MP2		EN2
	HF	MP	EN	MP	MP + F^{∞}	EN + F^{∞}
E_0	−77.919	−0.1307	−0.1535	−0.1326	−0.1594	−0.2141
$\epsilon_1(\Gamma)$	−12.96	−12.04	−11.79 (10%)	−11.91	−11.87	−11.48 (13%)
$\epsilon_2(\Gamma)$	−10.97	−10.80	−10.73 (2%)	−10.78	−10.77	−10.66 (3%)
$\epsilon_3(\Gamma)$	4.31	3.40	3.11 (39%)	3.39	3.25	2.51 (42%)
$\epsilon_4(\Gamma)$	4.85	3.92	3.63 (34%)	4.06	3.90	3.49 (39%)
$\epsilon_1(\frac{6}{7}X)$	−13.22	−11.84	−11.45 (15%)	−11.73	−11.65	−11.13 (19%)
$\epsilon_2(\frac{6}{7}X)$	−12.14	−10.78	−10.40 (17%)	−10.68	−10.61	−10.11 (20%)
$\epsilon_3(\frac{6}{7}X)$	7.25	6.41	6.11 (19%)	6.41	6.27	5.30 (37%)
$\epsilon_4(\frac{6}{7}X)$	8.19	7.43	7.16 (14%)	7.52	7.41	6.80 (20%)
Gap	15.28	14.20	13.84 (10%)	14.17	14.02	13.17 (16%)

same holds for deep-lying hole levels. In the case of the $(C_2H_4)_7$ ring in DZ basis, intruder states were observed for the valence lines, once the deep-lying levels are included in the model space. In Fig. 13 the LMP2(3) correction to the HF results (solid) of two of the upper valence lines are indicated as dotted lines. This time, all $(N-1)$-electron determinants had been included in the model space. Clearly, the correlation correction is severely overestimated as a consequence of some dangerously small energy denominators. To meet this difficulty, the theory of intermediate Hamiltonians assembles these troublesome states in an intermediate model space. Thus a knowledge of their correlation corrections is sacrificed in favor of calculating their effect on the correlation corrections of the main model space. To be specific, we recalculated the valence lines with an intermediate Hamiltonian based on Eqs. (27), (28), and (29), again on the LMP2(3) level. The result has been added as dot-dashed lines in Fig. 13. As shift parameter we used 30 au in Eq. (31). Owing to this shift, the strong coupling is suppressed and the results are converged, as can be seen in Fig. 13. However, in the present case the effect of the deep-lying levels is minute and a simple cut-off in the energy, as applied to the effective Hamiltonian in the previous two sections, does not constitute a significant approximation.

4 Conclusion

In conclusion, a size-consistent multi-reference method has been realized to calculate the correlation corrections of the IP and EA or, put another way, the "quasi band-structure", of cyclic periodic systems. The decisive aspect of the approach presented is the use of local HF orbitals apt to reduce the correlation space to a finite environment of the central cell, so that the method is applicable to infinite systems as well. The approach is based on the theory of the generalized Bloch Effective Hamiltonian which has been constructed to second order. The additional perturbation due to the use of non-canonical orbitals has been taken into account up to third order.

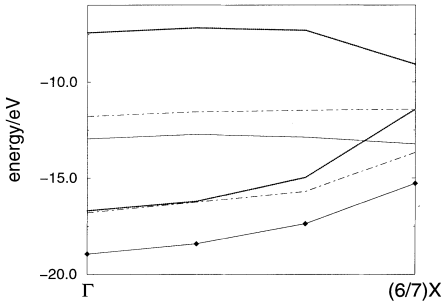

Fig. 13. Intruder-state effects for two of the upper valence lines. The LMP2(3) results as obtained with an effective Hamiltonian where all $(N-1)$-electron determinants were included in the model space are shown as *bold lines*. They give a far too large correction to the HF results (*solid lines*) as a consequence of the intruder states. The intermediate Hamiltonian leads to the improved calculation, shown as *dot-dashed lines*

The summation of certain classes of diagrams up to infinity both for the localization as well as for the Coulomb perturbation, and the relation of this procedure to the EN partitioning of the Hamiltonian were studied. Based on the theory of intermediate Hamiltonians, suggestions were put forth to treat the intruder state problem. All diagrams and necessary changes to some of them according to the type of theory employed were given. Finally, two ring systems, $(C_2H_4)_{13}$ and $(C_2H_4)_7$ with polyethylene geometry for the unit cell, served as test systems. The EN and third-order localization contributions gave significant contributions on top of the MP2 results. Subject to the basis set constraints, the corrections were found to be reasonable in their order of magnitude as compared to the literature for related systems.

Acknowledgements. This work has been made possible by a grant of the DAAD (Grant No. D/97/12548; M. A.), and of the European Community (Marie-Curie grant No. ERB–FMC–ICT–950119; P. R.). Computer time, provided by the Max-Planck-Institute in Dresden, is also gratefully acknowledged, as well as critical discussions with J.-L. Heully. The Laboratoire de Physique Quantique forms part of the UMR 5626 of the French Scientific Research Programme (CNRS).

Appendix A. diagrams of the effective Hamiltonian

The evaluation of the Bloch equation (Eq. 6) is considerably facilitated by Wick's theorem for operator products in normal form and the use of diagramatic representations as put forth in the book of Lindgren and Morrison [34]. Since our basis of local HF orbitals is orthonormal, this procedure is immediatly applicable. The notation follows that of Lindgren and Morrison, and is repeated in Fig. 14. The variables designate spin-space orbitals. Again only the case of particles is considered, the treatment of holes being completely analogous. Arrows pointing downwards generally represent core orbitals and have indices (a, b, c); those pointing upwards represent valence or virtual orbitals and are labeled (r, s, t). To address exclusively valence orbitals, a double arrow pointing upwards and lower-case Greek letters are used. To specify that an orbital is virtual, but not a valence orbital, a triangular arrow upwards is used together with upper case letters (R, S, T). In backfold diagrams, the backfolded double arrow is circled to remember that it is still a valence orbital, not a core orbital. Furthermore the convention $(ab\|rs) := (ab|rs) - (rb|as)$ is adopted together with the abbreviation $\Delta_{rs}^{ab} = \epsilon_a + \epsilon_b - \epsilon_r - \epsilon_s$.

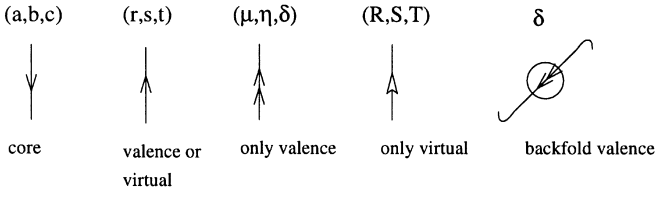

Fig. 14. Diagramatic notations as explained in the text

To second order, the diagrams for the matrix element

$$\langle \mu | H_{\text{eff}} - E_0 | \eta \rangle \tag{A1}$$

of the effective Bloch Hamiltonian are shown in Fig. 15. We note in passing that the first order simply consists of the off-diagonal Fock-operator elements. In all the diagrams these elements are just denoted by F, and it should be kept in mind that only these off-diagonal elements form part of the perturbation:

$$F_{ij} = \langle i | F | j \rangle (1 - \delta_{ij}) \tag{A2}$$

In the second order, the Fock matrix is invoked by the fifth diagram of Fig. 15 which assumes that some of the particle states

$$|T\rangle = c_t^\dagger |\Psi_{\text{scf}}\rangle \tag{A3}$$

have been attributed to the Q-space, as indicated by the use of capital letters and empty triangular arrows. The lower two diagrams originate from the fact that subtracting the ground-state energy E_0 in Eq. (A1) does not exactly cancel the corresponding diagrams of the effective Hamiltonian owing to the presence of the additional particle in state μ. Thus these diagrams are meant to represent only the EPV diagrams with respect to μ.

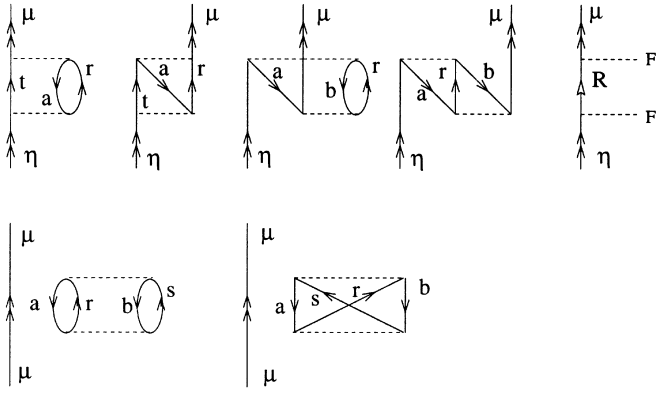

Fig. 15. All second-order diagrams of the effective Bloch Hamiltonian. The last two diagrams are meant to represent only the exclusion-principle-violating diagrams with respect to μ

The diagrams of the third order, which contain at least one Fock-operator element, are given in Figs. 16, 17, and 18. Again, the diagrams of Fig. 18 are to be taken care of only in as far as they constitute EPV diagrams with respect to μ. Note that, in third order, backfold diagrams appear for the first time. They are due to the second term of Eq. (8). A rough classification of these diagrams with respect to the second order consists in considering the diagrams of Fig. 16 as the natural extension of the first two diagrams in Fig. 15 and those in Fig. 17 as the ones originating from the next three diagrams of the second order, whereas the diagrams of Fig. 18 correspond to the last two diagrams of Fig. 15. As an example of the straightforward evaluation of these diagrams, we give the formula for the first two lines of Fig. 16:

$$\sum_{art} \frac{(t\eta|ra)}{\Delta_{tr}^{a\eta}} \left[\sum_s \frac{(\mu t \bar{\|} as) F_{sr}}{\Delta_{ts}^{a\eta}} + \sum_s \frac{(\mu s \bar{\|} ar) F_{st}}{\Delta_{sr}^{a\eta}} - \sum_b \frac{(br \bar{\|} \mu t) F_{ab}}{\Delta_{tr}^{b\eta}} + \sum_T \frac{(Tt \bar{\|} ar) F_{\mu T}}{\Delta_T^{\eta}} \right]$$
$$+ \sum_{art} \frac{(\mu t|ar)}{\Delta_{tr}^{a\eta}} \left[\sum_T \frac{(Tt \bar{\|} ar) F_{\eta T}}{\Delta_T^{\eta}} - \sum_\delta \frac{(ra \bar{\|} t\delta) F_{\delta\eta}}{\Delta_{tr}^{a\delta}} + \right]$$

where one has to make sure that EPV diagrams are avoided.

These diagrams form the basis of the LMP2(3) program, the third order being bracketed since we neglected the terms with three Coulomb interactions. The capital "L" in the abbreviation reminds us that a localized basis is used.

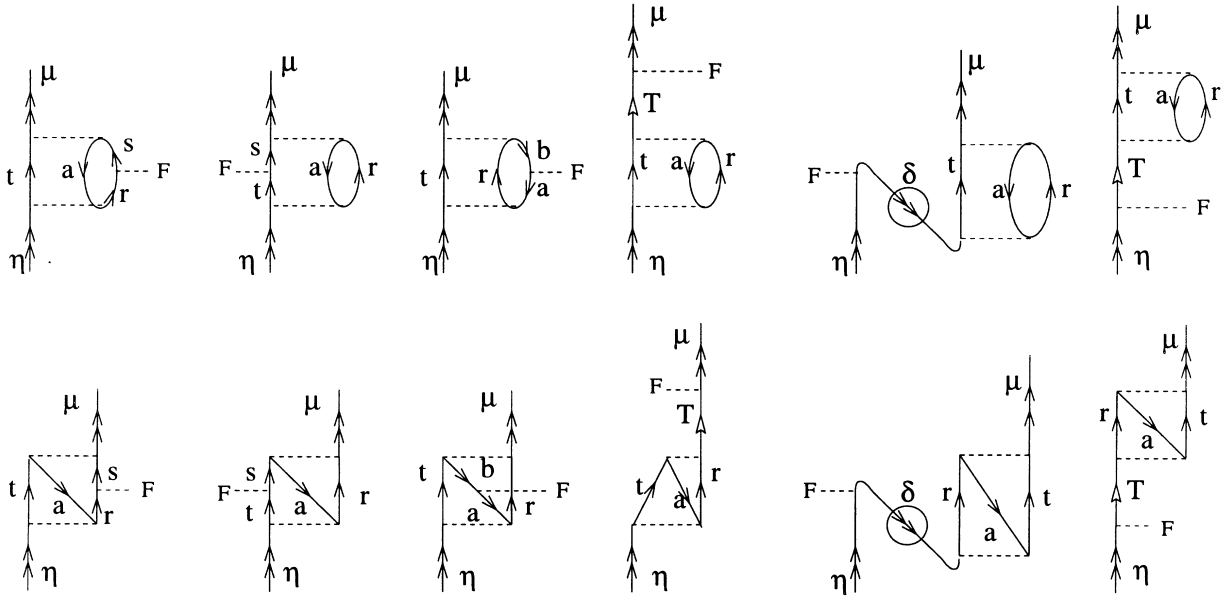

Fig. 16. Diagrams of $H_{\text{eff}}^{(3)}$ originating from the first two diagrams of Fig. 15

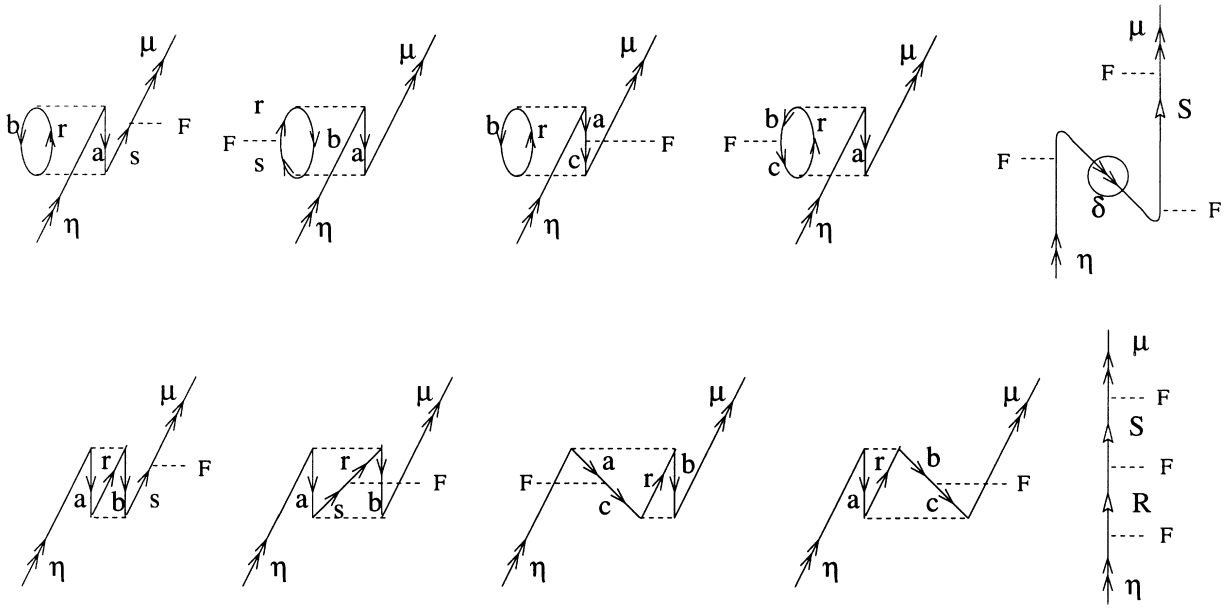

Fig. 17. Diagrams for the off-diagonal elements of $H_{\text{eff}}^{(3)}$ originating from diagrams three to five of Fig. 15. The *last column* gives the triple-F diagrams (on-diagonal and off-diagonal elements)

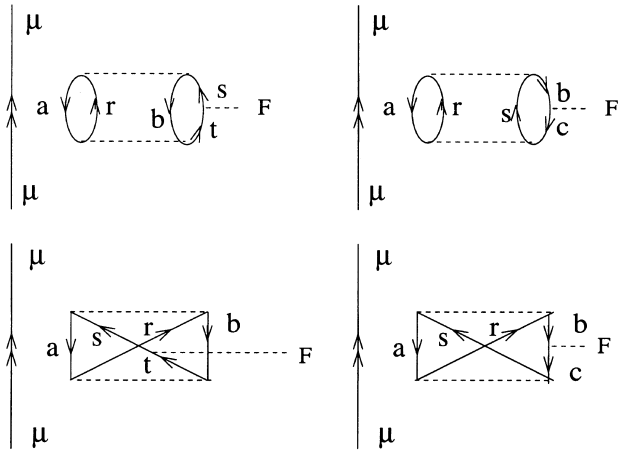

Fig. 18. Diagrams of $H_{\text{eff}}^{(3)}$ originating from the ground-state energy expression

References

1. Pulay P, Saebø S (1986) Theor Chim Acta 69: 357
2. Hampel C, Werner H-J (1996) J Chem Phys 104: 6286
3. Fink K, Staemmler V (1995) J Chem Phys 103: 2603
4. Kunz AB (1991) Phys Rev B 43: 9228
5. Stollhoff G, Fulde P (1980) J Chem Phys 73: 4548
6. Förner W (1992) Int J Quantum Chem 43: 221
7 Stoll H (1992) Phys Rev B 46: 6700
8 Paulus B, Fulde P, Stoll H (1995) Phys Rev B 51: 10572
9. Paulus B, Fulde P, Stoll H (1996) Phys Rev B 54: 2556
10. Kalvoda S, Paulus B, Fulde P, Stoll H (1997) Phys Rev B 55: 4027
11. Paulus B, Shi F-J, Stoll H (1997) J Phys Condens Matter 9: 2745
12. Albrecht M, Paulus B, Stoll H (1997) Phys Rev B 56: 7339
13. Doll K, Dolg M, Fulde P, Stoll H (1995) Phys Rev B 52: 4842
14. Doll K, Dolg M, Stoll H (1996) Phys Rev B 54: 13529
15. Doll K, Dolg M, Fulde P, Stoll H (1997) Phys Rev B 55: 10282
16. Doll K, Stoll H (1997) Phys Rev B 56: 10121
17. Gräfenstein J, Stoll H, Fulde P (1993) Chem Phys Lett 215: 610
18. Gräfenstein J, Stoll H, Fulde P (1997) Phys Rev B 55: 13588
19. Förner W, Knab R, Čižek J, Ladik J (1997) J Chem Phys 106: 10248
20. Borrmann W, Fulde P (1987) Phys Rev B 35: 9569
21. Vracko-Grobelsik M, Liegener CM, Ladik J (1990) Int J Quantum Chem 37: 241
22. Sun J-Q, Bartlett RJ (1996) J Chem Phys 104: 8553
23. Sun J-Q, Bartlett RJ (1997) J Chem Phys 106: 5554
24. Sun J-Q, Bartlett RJ (1997) J Chem Phys 107: 5058
25. Daudey JP (1974) Chem Phys Lett 24: 574
26. Rubio J, Povill A, Malrieu J-P, Reinhardt P (1997) J Chem Phys 107: 10044
27. Reinhardt P, Malrieu J-P, Povill Á, Rubio J (1998) Int J Quantum Chem (in press)
28. Reinhardt P, Malrieu J-P, J Chem Phys (in press)
29. Sano T, Matsuoka O (1996) Bull Chem Soc Jpn 69: 2195
30. Shukla A, Dolg M, Stoll H, Fulde P (1996) Chem Phys Lett 262: 213
31. Shukla A, Dolg M, Stoll H, Fulde P (1998) Phys Rev B 57: 1471
32. Shukla A, Dolg M, Stoll H, Fulde P (unpublished)
33. Kapuy E, Csépes Z, Kosmutza C (1983) Int J Quantum Chem 23: 981
34. Lindgren I, Morrison J (1985) Atomic many body theory. Springer, Berlin Heidelberg New York
35. Malrieu J-P, Durand P, Daudey J-P (1985) J Phys A Math Gen 18: 809
36. Sánchez-Marín J, Nebot-Gil I, Malrieu J-P, Heully JL, Maynau D (1997) Theor Chim Acta 95: 215
37. Heully J-L, Evangelisti S, Durand P (1995) J Phys II 5: 63
38. Cave RJ, Davidson ER (1988) J Chem Phys 89: 6798
39. Lepetit M-B, Malrieu J-P (1993) Chem Phys Lett 208: 503
40. Assfeld X, Almlöf JE, Truhlar DG (1995) Chem Phys Lett 241: 438
41. Gadea X, Maynau D, Malrieu J-P (1984) Int J Quantum Chem 26: 1
42. Forster P, Gschwind R, Haselbach E, Klemm U, Wirz J (1980) Nouv J Chim 4: 365
43. Szabo A, Ostlund NS (1996) Modern quantum chemistry. Dover, New York

44. Yaris R (1974) Chem Phys Lett 24: 386
45. König G, Stollhoff G (1989) J Chem Phys 91: 2993
46. Karpfen A (1981) J Chem Phys 75: 238
47. (a) Dovesi R, Pisani C, Roetti C, Causa M, Saunders VR (1989) CRYSTAL88; quantum chemistry program exchange, program No. 577. Indiana University, Bloomington, Ind.; (b) Dovesi R, Saunders VR, Roetti C (1992) CRYSTAL92 user document. University of Turin, Italy, and SERC Daresbury Laboratory, Daresbury, UK; (c) Dovesi R, Saunders VR, Roetti C, Causa M, Harrison NM, Orlando R, Apra E (1996) CRYSTAL95 user's manual. University of Turin, Italy
48. (a) Huzinaga S (1965) J Chem Phys 42: 1293; (b) Huzinaga S (1971) Approximate atomic functions. University of Alberta, Canada
49. Suhai S (1983) Int J Quantum Chem 23: 1239
50. Suhai S (1992) Int J Quantum Chem 42: 139
51. Suhai S (1986) J Chem Phys 84: 5071